Revista Mexicana de Astronomía y Astrofísica, **42**, 273–289 (2006)

SAN PEDRO MÁRTIR MID-INFRARED PHOTOMETRIC SYSTEM

L. Salas,[1] I. Cruz-González,[2] and M. Tapia[1]

Received 2005 September 21; accepted 2006 June 30

RESUMEN

Con el objetivo de definir el Sistema Fotométrico para el Mediano-Infrarrojo de San Pedro Mártir, se realizaron observaciones de estrellas de calibración bien estudiadas con la cámara del mediano-infrarrojo CID-BIB (2 − 28 μm) del Observatorio Astronómico Nacional, durante 9 temporadas de observación en 2000 a 2005. Se utilizó un conjunto de 9 filtros, los de la serie de "silicatos" SiN, SiO, SiP, SiQ, SiR, SiS, el filtro de banda ancha N (10.8 μm), y los filtros angostos QH2 (17.15 μm) y Q2 (18.7 μm), para determinar los coeficientes de extinción y los puntos cero en magnitud. Las correcciones por extinción atmosférica se llevaron a cabo mediante el uso de aproximantes de Padé, y los coeficientes involucrados se obtuvieron mediante una relacion lineal con el coeficiente de extinción a baja masa de aire. Se presentan y comparan las curvas de transmisión atmosférica de SPM y los coeficientes de extinción con los del sitio astronómico Mauna Kea. Utilizando un conjunto de fuentes IRAS LSR observadas con el CID-BIB se encuentran terminos de color.

ABSTRACT

With the goal of defining the San Pedro Martir Mid-infrared Photometric System (SPM-MIR), observations of well-defined calibration stars were carried out on 9 photometric runs from 2000 to 2005. The mid-infrared (2 − 28 μm) camera CID-BIB of the Observatorio Astronómico Nacional was used. A set of 9 filters, the "silicate" series SiN, SiO, SiP, SiQ, SiR, SiS, the broad-band N (10.8 μm) filter, and the narrow-band QH2 (17.15 μm) and Q2 (18.7 μm), was used to derive the extinction coefficients and zero magnitude points. Atmospheric extinction corrections were carried out making use of Padé approximants and we found a linear dependence on the parameters with the low air mass extinction coefficient. The atmospheric transmission curves and extinction coefficients of SPM were compared with those obtained for the Mauna Kea site. Color terms were derived using a set of IRAS LSR sources observed with the CID-BIB.

Key Words: **INSTRUMENTATION: PHOTOMETERS — SITE TESTING — STARS: FUNDAMENTAL PARAMETERS — TECHNIQUES: PHOTOMETRIC**

1. INTRODUCTION

The CID ("Cámara Infrarroja Doble") or Dual Infrared Camera, was designed for the 2.12 m telescope of the Observatorio Astrónomico Nacional in San Pedro Mártir (OAN/SPM), Baja California (México). The system consists of separate camera and camera/spectrograph that operate in two different regions of the IR spectrum, the CID-BIB for the mid-infrared (6–28 μm) and the CID-InSb for the near-infrared (1–5 μm). The CID-BIB, which is the instrument used in this paper, has a Boeing BIB 128×128 Si:As detector which is sensitive from 2 to 28 μm. The camera plate scale is 0.55″/pix on the detector (about half the diffraction spot) and covers

[1]Instituto de Astronomía, Universidad Nacional Autónoma de México, Ensenada, B. C., México.
[2]Instituto de Astronomía, Universidad Nacional Autónoma de México, México, D. F., México.

$64'' \times 64''$ on the sky. A detailed description of the two CID instrumental setups is presented in Salas et al. (2003). After the initial commissioning in 1999 the detector noise was greatly reduced and optimized (see Sohn et al. 2001 for details), and the CID-BIB began astronomical observations in 2000. Mid-infrared observations of calibration stars have been done on 9 photometric runs from 2000 to 2005, with the main goal of defining the San Pedro Mártir Mid-Infrared Photometric System (SPM-MIR).

2. FILTER SET

The CID-BIB consists of a set of nine filters described in Table 1, which includes 6 narrow-band "silicate" OCLI filters (SiN, SiO, SiP, SiQ, SiR, SiS) in the 10 μm window, supplemented by adequate block filters, a broad-band OCLI N filter and two 20 μm window narrow-band filters acquired from the University of Reading through a universities consortium.

The total response of the filter system, following Tokunaga & Vacca (2005), is given by

$$S(\lambda) = T_A(\lambda)\, T_F(\lambda)\, QE(\lambda)\,, \tag{1}$$

where $T_A(\lambda)$ is the atmospheric transmission, $T_F(\lambda)$ is the filter response times the action of the corresponding block filter, and $QE(\lambda)$ is the detector quantum efficiency.

To estimate the atmospheric transmission we use the AFGL code MODTRAN3 (Version 1.3) (Berk, Bernstein, & Robertson 1989) as indicated in Young, Milone, & Stagg (1994) with values appropriate for the San Pedro Mártir (SPM) site with a median water vapor content of 3 mm (Hiriart et al. 1997) at zenith. The filter transmission and detector quantum efficiency are taken from the manufacturers. Figure 1 shows the resulting filter response and the individual contributions to $S(\lambda)$ of $T_F(\lambda)$, blockings, $QE(\lambda)$, and $T_A(\lambda)$ for SPM.

The mean wavelength λ_0 and isophotal wavelength λ_{iso} (Golay 1974; Tokunaga & Vacca 2005) for each filter can be obtained as:

$$\lambda_0 = \frac{\int \lambda S(\lambda) d\lambda}{\int S(\lambda) d\lambda}\,, \tag{2}$$

and

$$F_\lambda(\lambda_{iso}) = \frac{\int \lambda f_\lambda(\lambda)\, S(\lambda)\, d\lambda}{\int \lambda\, S(\lambda)\, d\lambda}\,, \tag{3}$$

where $F_\lambda(\lambda_{iso})$ equals the weighted average of the monochromatic flux $\langle f_\lambda(\lambda)\rangle$ in the bandwidth. To define a particular set of λ_{iso}, we follow the procedure of Cohen et al. (1992a), setting f_λ to the calibrated spectral energy distribution of a model of Vega calculated by Kurucz.

Table 1 shows the calculated mean λ_0 and isophotal λ_{iso} wavelengths. We also calculate the pivot wavelength λ_p such that

$$F_\nu(\lambda_p) = F_\lambda(\lambda_p)\,\frac{\lambda_p^2}{c}\,, \tag{4}$$

for each filter, and the width of the filter $\Delta\lambda$ from the second moment of the filter response (assuming a square equivalent filter). Finally, the mean (isophotal) flux of the Vega model is converted to Jy to complement our definition of the 0th magnitude of the system.

3. LIST OF STANDARDS

In a series of papers, Cohen and collaborators (Cohen et al. 1992a, 1992b, 1995, 1996, 1999, herein CC) have defined a grid of radio-metrically calibrated standard stars. We have taken 7 stars from this list to calibrate the SPM-MIR system (see Table 2).

For each star we calculate the expected isophotal flux (Eq. 3) from the irradiance spectra given by CC; then convert to F_ν at the pivot wavelength of the filter and calculate the magnitude relative to the Vega model taken as 0.

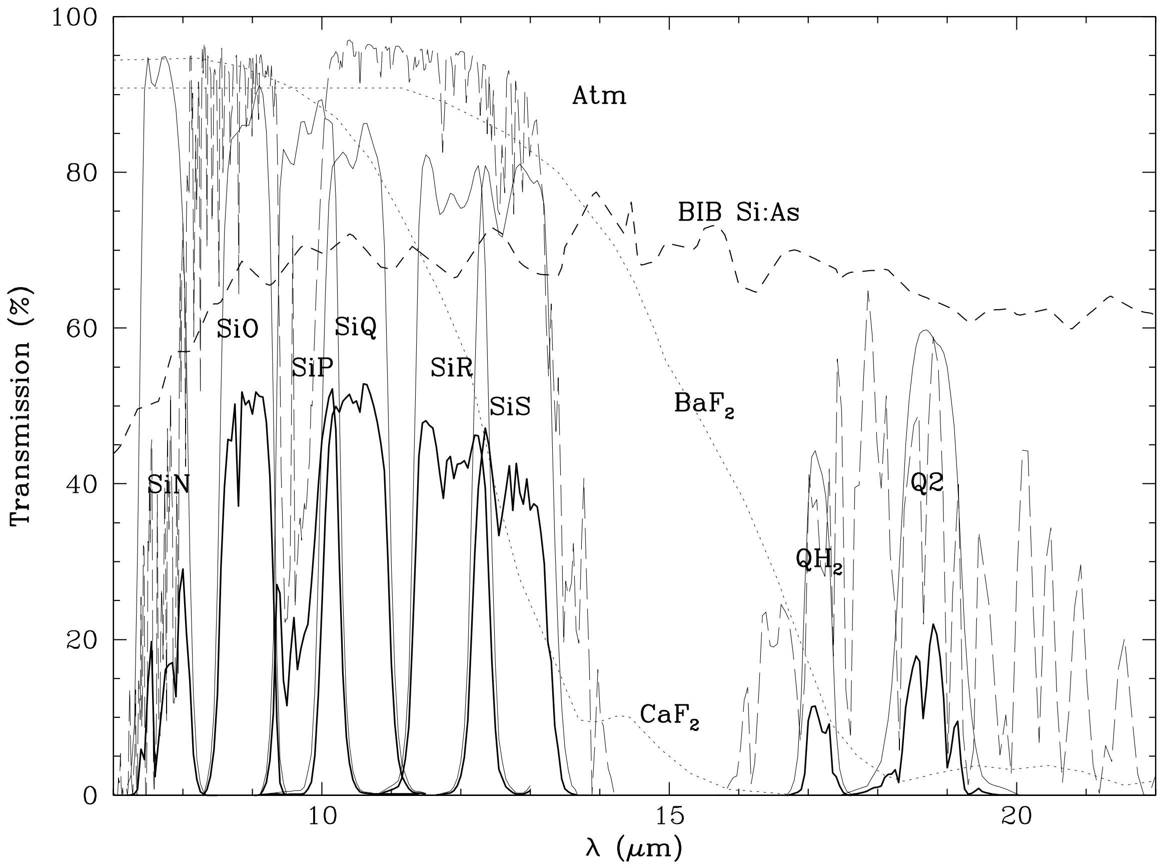

Fig. 1. Filter response. Solid thin line: original filter transmission ($T_F(\lambda)$); dotted line: block filter transmission; short dashed line: BIB Si:As detector QE; long dashed line: Atmospheric transmission (3 mm H_2O SPM); solid thick line: total response $S(\lambda)$ for each filter. For clarity the wide filter N is not shown.

TABLE 1

SPM-MIR SYSTEM

Filter	Block	λ_0 μm	λ_{iso} μm	λ_p μm	$\Delta\lambda$ μm	0 mag Jy
SiN	CaF_2	7.83	7.85	7.82	0.72	61.85
SiO	CaF_2	8.92	8.90	8.92	0.80	48.08
SiP	BaF_2	9.90	9.90	9.90	1.03	39.35
SiQ	BaF_2	10.49	10.45	10.49	1.04	35.08
SiR	BaF_2	11.86	11.85	11.86	1.20	27.58
SiS	BaF_2	12.70	12.70	12.69	1.20	24.11
N	BaF_2	10.80	10.45	10.69	5.28	36.48
QH2	···	17.15	17.15	17.15	0.46	13.33
Q2	···	18.70	18.70	18.70	1.01	11.20

TABLE 2

CC'S RADIOMETRICALLY CALIBRATED STARS

Filter	α Tau mag	α Boo mag	β And mag	β Gem mag	β Peg mag	μ UMa mag	α CMa mag
SiN	−2.97	−3.11	−2.00	−1.21	−2.37	−0.83	−1.35
SiO	−2.95	−3.11	−1.98	−1.21	−2.38	−0.85	−1.35
SiP	−3.01	−3.16	−2.06	−1.22	−2.44	−0.93	−1.36
SiQ	−3.05	−3.18	−2.10	−1.22	−2.47	−0.97	−1.35
SiR	−3.06	−3.18	−2.12	−1.22	−2.49	−1.00	−1.35
SiS	−3.07	−3.18	−2.12	−1.22	−2.49	−1.00	−1.35
N	−3.00	−3.15	−2.04	−1.22	−2.43	−0.92	−1.35
QH2	−3.05	−3.17	−2.11	−1.23	−2.51	−1.00	−1.34
Q2	−3.06	−3.19	−2.12	−1.23	−2.52	−1.00	−1.34

4. ATMOSPHERIC CORRECTIONS

MIR extinction is dominated by a vast collection of molecular absorption lines, mainly from water vapor and ozone in the Earth's atmosphere. This creates a difficult problem for obtaining the extra-atmospheric flux F^0_λ.

The monochromatic extra-atmospheric flux f^0_λ is related to the flux at the exit pupil of the telescope by the simple solution of the transport equation $f^e_\lambda = f^0_\lambda e^{-\tau_\lambda}$, where the optical depth is given by the absorption coefficient $k_\lambda(\xi)$ as

$$\tau_\lambda = \int_0^{l_\circ} k_\lambda(\xi) dl \,, \tag{5}$$

integrated along direction $\vec{l}$ through the atmosphere, from the observatory's position ($l = 0$) to outside the atmosphere ($l = l_0$). If $\vec{l}$ is at an angle z to the normal $\vec{\xi}$ (i.e., $\cos z = d\xi/dl$), then for a plane-parallel approximation (small z), the τ_λ integral can be expressed in terms of the zenith optical depth as

$$\tau_\lambda = M\tau^0_\lambda \,, \tag{6}$$

where M is the air mass.

In this way, when we observe through a passband w, the flux is

$$F_\lambda = \langle f_\lambda(\lambda)\rangle = \int_w f_\lambda(\lambda) e^{-M\tau_\lambda} d\lambda \,, \tag{7}$$

and if τ_λ is either constant or a linear function of λ, it is possible to perform a change of variables to take M out of the integral. This gives rise to a linear extinction law (Bouguer) which allows us to obtain F^0_λ.

However, when observing through a pass-band that includes absorption lines, this is not strictly possible. At the wavelength where the monochromatic extinction is greater, the star's light is absorbed higher in the atmosphere, even undergoing complete obscuration before reaching the observatory. This gives rise to a non-linear extinction law, particularly in the $0 < M < 1$ region, where the extinction curves up, causing the true extra-atmospheric flux to be underestimated when a linear Bouguer extinction law is assumed. The amount of this defect is not constant, and depends on the color of the object being observed. This is known as the Forbes (1842) effect (see for example Young et al. 1994).

It has been shown that the best way to deal with this problem is by designing a set of filters that avoids the most compromising regions of the atmosphere, preferably with soft edges (e.g., Young et al. 1994; Milone & Young 2005, Tokunaga, Simons, & Vacca 2002). Nevertheless, appropriate parameterizations of the extinction curve have been proposed that allow good corrections, although they had been regarded as somehow impractical,

TABLE 3

FORBES EFFECT ERROR

Filter	T (K)	k_{12}	Δ	Filter	T (K)	k_{12}	Δ
SiN	1000	0.84	0.40	SiR	1000	0.08	0.001
SiN	50	0.54	0.24	SiR	50	0.08	0.002
SiO	1000	0.11	0.006	SiS	1000	0.18	0.010
SiO	50	0.11	0.006	SiS	50	0.22	−0.014
SiP	1000	0.39	0.19	QH2	1000	1.15	−0.054
SiP	50	0.21	0.11	QH2	50	1.19	0.02
SiQ	1000	0.07	0.008	Q2	1000	0.927	0.21
SiQ	50	0.06	0.002	Q2	50	0.944	0.25

due to the large number of parameters involved and the fact that the $0 < M < 1$ region is un-observable for most applications. In this respect, Young et al. (1994) have analyzed a solution for the observed magnitude (m) as a function of M given in terms of Padé approximants:

$$m = \frac{a + (a + b_0 + b_1 C)\ (d_0 + d_1 C)\ M + c\ (d_0 + d_1 C) M^2}{1 + (d_0 + d_1 C) M}\,. \tag{8}$$

They have concluded that knowing the five parameters (b_0, b_1, c, d_0, d_1) allows one to reach milli-magnitude precision in the case of Johnson's JKLM filter set. The advantage of this particular parametrization is that all 5 parameters are color-independent and may be determined from atmospheric models and the filter transmission curves. Therefore, one can have an expression that relates the observed magnitude m at a given air mass (M) in terms of the extra-atmospheric magnitude (a) and the color of the source C.

The CID filter set was not designed to avoid the Forbes effect. In particular, the SiN, SiP, Q2, QH2, and N filters are most affected, mainly by water bands and, in the case of SiP, by ozone's absorption at 9.7 μm. In Figure 2 we illustrate this problem for the SiP pass-band.

Following the procedure in Tokunaga et al. (2002), we have taken the MODTRAN3 atmospheric transmission models for a water vapor content of 3 mm, calculated τ^0_λ from them, and scaled it for different values of M, from 0 to 3. This is fine for $M > 1$ (see Eq. 6) and for the point $M = 0$ (where $\tau_\lambda = 0$), but is not necessarily true in the interval $0 < M < 1$, particularly for ozone. However, we are only interested in the outcome value at $M = 0$ and the curve at $M > 1$ which should be accurately described. The resulting absorption spectra are shown as dashed lines in Fig 2a. We note that the atmospheric transmittance $T_A(\lambda)$ decreases as M increases. We also show the transmitted flux from a hypothetical object, a Rayleigh-Jeans (RJ) continuum (thin line), which gets increasingly depressed. When we integrate over the SiP filter (solid line), we may calculate the magnitude of the object as a function of M. This is shown next in Fig. 2b as crosses. The comparison to a linear extinction law (dotted line fitted to the $1 < M < 2$ region) shows that an error Δ would be made at $M = 0$ due to the Forbes effect as was mentioned. We have calculated the magnitude of Δ (Table 3) for every narrow-band filter in the set and two hypothetical objects: black bodies at 1000 and 50 K.

As can be seen, the effect is small ($< 1\%$) for the SiO, SiQ, SiR, SiS filters. Elsewhere, the effect reaches tenths of magnitude levels, and a strong dependence on the color of the source is evident. Also listed in this table is the linear extinction coefficient k_{12} that one would derive from observations between M =1 and 2. This coefficient also varies, making it impossible to use a hot calibration source for a cold problem object.

Following the suggestion of Young et al. (1994), we have found the values of the parameters for the Padé approximant (Eq. 8) for the extinction curve. In doing so, we defined the color coefficient C as

$$[8.9] - [18.7] \;=\; -2.5\,\log\left(\frac{F_\lambda(8.9)}{F_\lambda(18.7)}\right) \;+\; 1.58\,. \tag{9}$$

An example of such a fit is shown in Fig. 2b (solid line). When the color of the source is close to zero (and close also the RJ limit), only three parameters (b_0, c, d_0) need to be adjusted. These are related to the

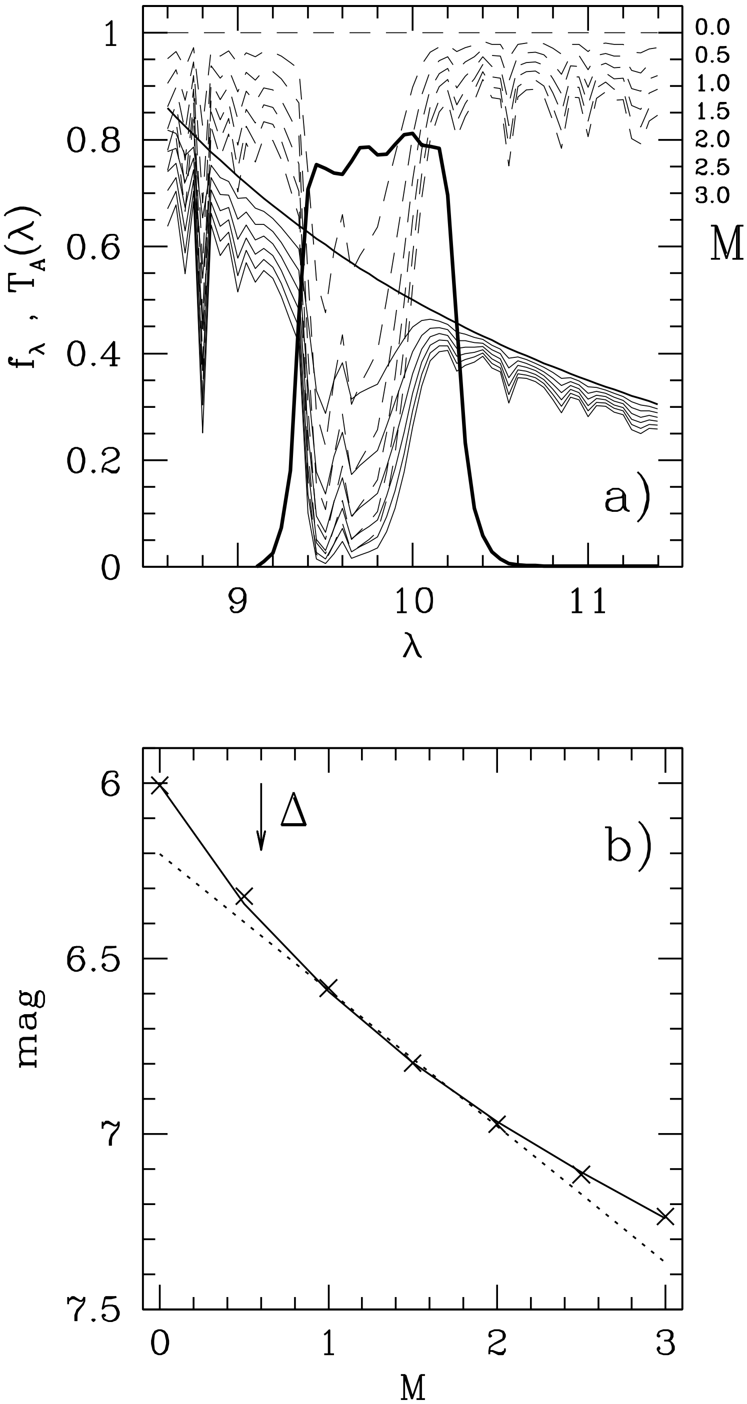

Fig. 2. Forbes effect. (a) Atmospheric transmission $T_A(\lambda)$ (dashed line) for increasing air-mass M from 0 to 3, attenuates an observed continuum source f_λ (thin lines). The spectral region corresponds to the SiP filter (solid line). (b) Magnitude obtained by integrating the transmitted flux over the filter's response (crosses) for each air-mass M. An error Δ is made from the extrapolation of a linear (Bouguer) extinction law (dotted line). A fit by Padé approximants (solid line) may correct this problem.

TABLE 4

FITS TO PADÉ APPROXIMANTS

Filter	$b0$[a]		$b1$		c		$d0$		$d1$		Residual Error
	m	ord	m	ord	m	ord	m	ord	m	ord	(mag)
SiN	7.2159	−2.1010	−0.1426	0.0616	0.0000	0.3200	0.0000	0.4000	0.0000	−0.0060	0.046
SiO	0.3060	−0.0049	−0.0112	0.0010	1.0026	−0.0007	0.0000	5.0000	0.0000	0.0000	0.004
SiP	3.6657	0.2922	0.0000	−0.0520	0.0000	0.1300	0.0000	0.4608	0.0000	0.0010	0.020
SiQ	0.9638	0.0129	0.0105	−0.0032	1.0161	−0.0021	0.0000	1.0000	0.0000	0.0000	0.007
SiR	1.0185	−0.0008	0.0265	0.0008	0.9967	0.0004	0.0000	1.0000	0.0000	−0.0100	0.004
SiS	1.2754	0.0100	−0.0046	0.0013	1.0018	−0.0005	0.0000	0.8333	0.0000	0.0170	0.015
QH2	2.2810	−0.4484	0.0061	0.0165	1.0013	−0.0011	0.0000	0.5000	0.0000	−0.0010	0.021
Q2	2.8203	−0.0593	0.0110	0.0073	0.7500	0.0609	0.0000	0.5000	0.0000	−0.0020	0.0047
N	2.3560	0.1896	0.1174	0.0230	0.8824	−0.0531	0.0000	0.5263	0.0000	0.0060	0.085

[a]e.g., $b0 = mk_{12}$+ord.

ordinate, the slope at large air mass and the inflection point of the curve. The rest of the parameters become important for redder colors. To fit those, we have explored 21 sources with effective temperatures between 30 and 3000 K taken at logarithmic intervals of 0.1 dex. In the end, the 5 parameters that minimize the mean quadratic error of the curve fit in the interval $1 < M < 2$ for all the 21 sources simultaneously, are selected. With this we confirm that the parametrization proposed by Young et al. (1994) is powerful enough to attain the magnitude of the Forbes effect in sources with colors that vary up to 30 magnitudes.

Next, we changed the atmospheric model (calculated with MODTRAN3) to different values of water vapor content, selected from the following: 0.25, 0.5, 1, 2, ..., 10 mm. For each atmospheric model we obtained the set of 5 parameters for Eq. 8 as described above. Additionally, for each model we collected the value of the extinction coefficient k_{12} (for $1 < M < 2$), that one would obtain for a hot source (3000 K, well in the RJ limit). It is interesting to note that in all cases and for all the filters in our set, the Padé parameters correlate linearly with k_{12}, as can be seen in Figure 3. In Table 4 we present the results of such linear fits. This allows us to calculate the 5 parameters for the Padé approximant and correct the Forbes effect, starting from a given value of k_{12} obtained from observations of a hot source (RJ limit) between 1 and 2 air-masses. The residual error that can be expected from this procedure is also listed in Table 4. This error comes mainly from the difficulty of obtaining a good fit for the very cold sources (< 60 K). With this we have now an excellent correction (< 1%) for the SiO, SiQ, SiP, SiR, SiS, Q2 filters, a marginal one (<2%) for the SiP and QH2 filters, and a rather poor one (< 8%) for the SiN and N filters. However, this result should be taken with caution. Short term variations in the atmospheric water vapor content, or ozone, in the direction of the observed source, may render a different value of k_{12} and thus result in a correction value which is not appropriate.

5. OBSERVATIONS

The set of calibration stars were observed during 9 observing runs (May/00, Sep/00, Jan/01, Nov/01, May/02, Sep/02, Jun/03, Aug/04, Nov/05) with good observing conditions. The observing procedure was to observe each source in a sequence of three different telescope positions, with the secondary mirror oscillating at a frequency of 3 Hz and an amplitude of 20″, therefore generating on-and off-source images (typically 20 oscillations for the brightest stars). All six frames are recorded and reduced to obtain six different estimates of the object's flux. Then the average and standard deviation constitute a particular observation of the source. For the reduction we follow the procedure explained in the instrument user's manual `http://www.astrossp.unam.mx/indexspm.html`: first calculating median background for on- and off-source frames separately. The difference of backgrounds is then subtracted from each difference of on- minus off-source object's observation. Each quadruple difference so obtained, is flat-fielded by a corresponding difference of on- or off-source observations of the sky at high air mass minus low air mass, which has been normalized to one.

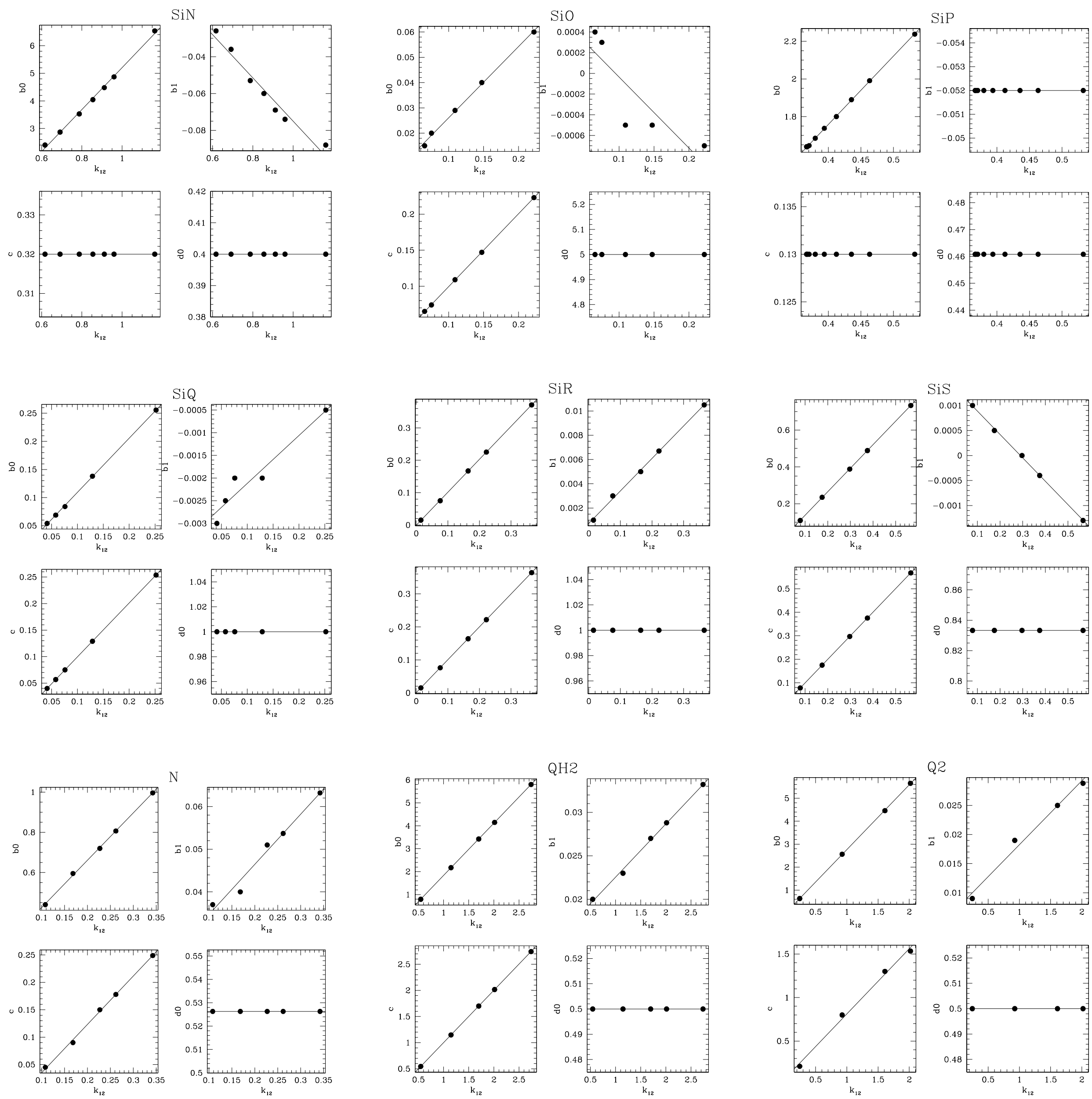

Fig. 3. Coefficients b_0, b_1, c, d_0 for the Padé approximants as a function of extinction coefficient k_{12} for a RJ continuum. They are shown for each one of the CID filters.

We have constrained our observations to low air masses ($M < 2$) and thus we use a linear fit to derive extinction coefficients k_{12} from observations of a particular source through different air masses. From these coefficients, the parameters (b_0, b_1, c, d_0, d_1) involved in the Padé approximants for the extinction curve (Table 4) are calculated. We add a zero point Z to the instrumental magnitude and the resulting magnitude is corrected by means of Equation 8 to obtain the extra-atmospheric magnitude (the a term in Eq. 8). The zero point is then adjusted in order to match the flux of the appropriate standard star (from Table 2).

Average values for Z and k_{12} for each run are presented in Tables 5 and 6, together with mean values for all the runs. The standard deviations (s.d.) quoted for the mean zero points reflect variations of these between

TABLE 5

MEASURED EXTINCTION COEFFICIENTS k_{12}

RUN	SiN	SiO	SiP	SiQ	SiR	SiS	N	QH2	Q2
May/00	···	···	···	···	···	0.22±.03	0.28±.08	···	···
Sep/00	···	0.15±.04	0.23±.02	···	0.30±.10	0.20±.05	···	···	···
Jan/01	···	0.05±.05	0.19±.05	···	···	0.09±.03	···	···	···
Nov/01	···	0.16±.05	0.37±.12	···	···	0.19±.07	···	···	···
May/02	0.45±.05	0.18±.03	0.28±.02	···	0.10±.03	0.14±.02	···	0.60±.05	0.65±.05
Sep/02	0.55±.05	0.12±.02	0.21±.02	0.10±.05	0.11±.04	0.12±.02	···	0.80±.05	0.70±.10
Jun/03	0.54±.05	0.17±.05	0.30±.03	0.16±.04	0.15±.05	0.17±.05	···	0.80±.10	0.70±.15
Aug/04	0.58±.05	0.15±.05	0.34±.05	0.03±.10	0.05±.05	0.11±.05	···	0.80±.10	0.70±.10
Nov/05	0.59±.03	0.24±.03	0.37±.03	0.36±.05	0.35±.02	0.24±.04	0.28±.05	0.90±.10	0.95±.10
$< k_{12} >$(s.d.)	0.54(0.06)	0.15(0.05)	0.29(0.07)	0.16(0.14)	0.18(0.12)	0.16(0.05)	0.28(0.00)	0.77(0.11)	0.72(0.08)

TABLE 6

ZERO POINTS AT AIR MASS = 0

RUN	SiN	SiO	SiP	SiQ	SiR	SiS	N	QH2	Q2
May/00	11.14	11.47	11.35	11.25	11.06	10.84	13.07	···	···
Sep/00	10.84	11.86	11.81	11.84	11.58	11.14	13.52	···	···
Jan/01	···	11.95	11.90	···	11.62	11.46	···	···	···
Nov/01	···	12.01	11.94	···	11.65	11.48	···	···	···
May/02	11.25	11.99	11.77	···	11.50	11.37	···	7.96	9.42
Sep/02	11.31	11.95	11.82	11.73	11.52	11.24	···	7.58	8.68
Jun/03	11.73	12.12	11.97	11.77	11.81	11.54	···	8.33	9.84
Aug/04	11.61	12.01	11.99	11.47	11.56	11.35	···	7.87	9.42
Nov/05	11.79	12.19	12.12	12.01	11.86	11.48	13.71	8.09	9.78
mean	11.38	11.95	11.85	11.68	11.57	11.32	13.43	7.97	9.40
(s.d.)	(0.35)	(0.20)	(0.22)	(0.27)	(0.23)	(0.22)	(0.33)	(0.28)	(0.44)

observing runs, while for the extinction coefficients the uncertainties in the individual determinations dominate.

We note that not all the stars were observed in all the observing runs. In each run at least either α Tau or α Boo were observed, and these two constitute our fundamental standards. These two standards were not observed simultaneously in any observing run, but stars from other lists (like μ Cep and α Her) have been observed with both fundamental standards and the photometry obtained for them coincides typically within 3%. We note that Vega (α Lyr) was not used for calibration, but only to check the consistency of the system. Vega is measured to be 0 within the measuring uncertainties of 5% typically, although in the Q2 filter it goes up to 20%. Also note that the largest deviations from the magnitudes given in Table 2 are for the star β And, which deviates $\sim$ 10% in most filters (an effect consistently checked in three observing runs).

Nevertheless, we have used all the measurements from the 9 observing runs to verify the consistency with the defining set of standards of Table 2. In Table 7 we report the standard errors of the differences between the measured magnitude and the values given in Table 2 for each filter. The number of stars that were observed in each filter is also indicated in the table. One can see that the magnitude values agree within the standard errors. In most cases these errors arise from measuring errors. However, in some cases we might have real differences from the values given by Cohen and collaborators (CC).

TABLE 7

COMPARISON TO CC'S LIST

Filter	Difference mag	Error mag	No. of Stars
SiN	0.010	0.044	7
SiO	−0.016	0.033	8
SiP	0.003	0.048	8
SiQ	0.011	0.064	5
SiR	0.008	0.048	8
SiS	0.014	0.042	8
N	0.013	0.034	5
QH2	0.077	0.108	7
Q2	0.067	0.093	7

TABLE 8

COMPARISON TO TOKUNAGA'S LIST OF STANDARD STARS

Filter	Difference mag	Error (s.d.) mag	No. of Stars
N	−0.029	0.163	9
Q (Q2)	0.012	0.164	9

During the same observing runs we also observed 10 of the standard stars given by Tokunaga (1986) in the filters N and/or Q. We compare these to our broad-band N and narrow-band Q2, respectively. The results of this photometric comparison show good agreement and are presented in Table 8. The measurements correspond to the bright standard stars β And, α Ari, α Tau, α Boo, α Sco, α Her, γ Aql, μ Cep, α Lyr, μ Uma, and α CMa.

For completeness, average magnitudes, standard errors and variations between different observing runs are presented in Table 9, for each of the 15 bright stars observed during the period 2000 to 2005.

6. COMPARISON TO MAUNA KEA

Mauna Kea is one of the best characterized sites in the world, especially in the infrared. It is therefore useful to compare it to San Pedro Mártir, which is also located in the Northern hemisphere and has proven to be an excellent site (see Cruz-González, Avila, & Tapia 2003). In Fig. 4, we present a comparison of the atmospheric transmission curves for both sites. The two curves for San Pedro Mártir were obtained using MODTRAN3, as described in § 2, for water vapor contents of 1 and 3 mm, respectively. The corresponding curve for Mauna Kea is for 1 mm and was calculated by E. Milone also using MODTRAN and presented in `http://www.gemini.edu/science/mkmodels/mk_absor.txt`. In Fig. 5 we compared the measured extinction coefficients (see Table 5) to the Mauna Kea measurements (Krisciunas et al. 1987). The 10 μm window filters have similar characteristics, while for the 20 μm window we compare two narrow-band SPM filters at 17.15 and 18.7 μm with a Q filter. Figures 4 and 5 are consistent and show that both sites have comparable atmospheric transmission in the mid-infrared. If we take the 3 mm water vapor content curve, the median SPM value (see Hiriart et al. 1997), one can see that Mauna Kea is better behaved in the bands affected by water vapor content, especially 7.7 and 20 μm. The other notable discordance is in the 9.8 μm band where the latitude difference, 19^o versus 31^o, increases the absorption due to ozone.

TABLE 9

AVERAGE MAGNITUDES OF BRIGHT STARS

	β And				α Ari				α Tau				μ Uma			
Filter	mag	err	var	N	mag	err	var	N	mag	err	var	N	mag	err	var	N
SiN	−1.91	0.03	0.04	5	···	···	···	0	−2.98	0.04	0.00	16	−0.78	0.17	···	2
SiO	−1.93	0.03	0.04	9	−0.71	0.03	0.02	5	−2.95	0.03	0.00	30	−0.89	0.01	···	1
SiP	−1.97	0.03	0.03	9	−0.73	0.04	0.03	4	−3.02	0.03	0.01	31	−0.94	0.03	···	2
SiQ	−2.01	0.07	0.02	6	···	···	···	0	−3.04	0.05	0.02	16	···	···	···	0
SiR	−2.00	0.07	0.06	7	···	···	···	0	−3.06	0.04	0.01	20	−1.00	0.05	···	1
SiS	−2.05	0.03	0.06	8	−0.72	0.06	0.06	4	−3.07	0.04	0.01	41	−1.00	0.02	···	1
N	−1.96	0.02	0.04	3	−0.78	0.04	···	2	−2.99	0.03	0.01	14	···	···	···	0
QH2	−2.01	0.10	0.15	2	···	···	···	0	−3.06	0.10	0.01	13	−1.07	0.02	···	1
Q2	−1.93	0.06	0.00	3	···	···	···	0	−3.06	0.16	0.01	14	−0.93	0.05	···	2

	α Aur				β Gem				α Boo				β Leo			
Filter	mag	err	var	N	mag	err	var	N	mag	err	var	N	mag	err	var	N
SiN	···	···	···	0	···	···	···	0	−3.11	0.11	0.00	11	1.80	0.21	···	2
SiO	−1.91	0.02	0.03	3	−1.24	0.01	···	1	−3.11	0.03	0.00	11	1.94	0.07	···	2
SiP	−1.92	0.02	0.03	4	−1.25	0.01	···	1	−3.16	0.03	0.00	9	2.22	0.34	···	1
SiQ	···	···	···	0	···	···	···	0	−3.18	0.07	···	3	···	···	···	0
SiR	···	···	···	0	−1.22	0.03	···	1	−3.18	0.03	0.00	9	1.90	0.18	···	2
SiS	−1.88	0.03	0.01	3	−1.19	0.02	···	1	−3.18	0.03	0.00	9	2.34	0.13	···	1
N	···	···	···	0	···	···	···	0	−3.15	0.02	···	3	···	···	···	0
QH2	···	···	···	0	···	···	···	0	−3.17	0.10	···	6	···	···	···	0
Q2	···	···	···	0	···	···	···	0	−3.19	0.45	···	6	···	···	···	0

	α Sco				α Her				γ Aql				μ Cep			
Filter	mag	err	var	N	mag	err	var	N	mag	err	var	N	mag	err	var	N
SiN	−4.35	0.15	···	2	−3.75	0.05	0.01	15	−0.78	0.11	0.17	4	−2.75	0.06	0.11	15
SiO	−4.66	0.04	···	2	−3.73	0.03	0.03	20	−0.67	0.04	0.05	10	−3.50	0.03	0.03	27
SiP	−4.87	0.03	···	2	−3.86	0.03	0.05	21	−0.71	0.03	0.06	10	−4.15	0.03	0.04	27
SiQ	−5.06	0.13	···	2	−3.94	0.05	···	5	−0.69	0.01	···	1	−4.41	0.04	0.04	12
SiR	−5.04	0.05	···	2	−3.98	0.03	0.03	18	−0.76	0.04	0.07	5	−4.20	0.04	0.05	17
SiS	−5.11	0.09	···	3	−3.98	0.05	0.02	23	−0.74	0.11	0.04	12	−4.02	0.04	0.04	27
N	−4.98	0.07	···	4	−3.93	0.03	···	3	−0.71	0.07	···	7	−3.95	0.02	0.03	15
QH2	···	···	···	0	−4.12	0.10	0.03	16	−0.78	0.19	···	4	−4.66	0.14	0.07	12
Q2	···	···	···	0	−4.18	0.09	0.00	16	−0.96	0.14	···	3	−4.89	0.07	0.07	12

	β Peg				α Lyr				α CMa			
Filter	mag	err	var	N	mag	err	var	N	mag	err	var	N
SiN	−2.36	0.05	···	3	−0.07	0.05	···	1	−1.35	0.04	···	3
SiO	−2.45	0.03	0.03	14	−0.01	0.05	···	2	−1.37	0.01	···	2
SiP	−2.50	0.03	0.05	13	0.08	0.01	···	2	−1.38	0.03	···	3
SiQ	−2.42	0.04	···	2	···	···	···	0	−1.45	0.05	···	3
SiR	−2.49	0.05	0.07	4	0.02	0.08	···	2	−1.42	0.04	···	3
SiS	−2.55	0.03	0.04	13	0.08	0.07	···	2	−1.36	0.03	···	3
N	−2.44	0.04	···	4	···	···	···	0	−1.37	0.03	···	2
QH2	−2.34	0.21	···	1	0.08	0.27	···	1	−1.07	0.35	···	1
Q2	−2.57	0.04	···	1	0.22	0.16	···	1	−1.31	0.12	···	1

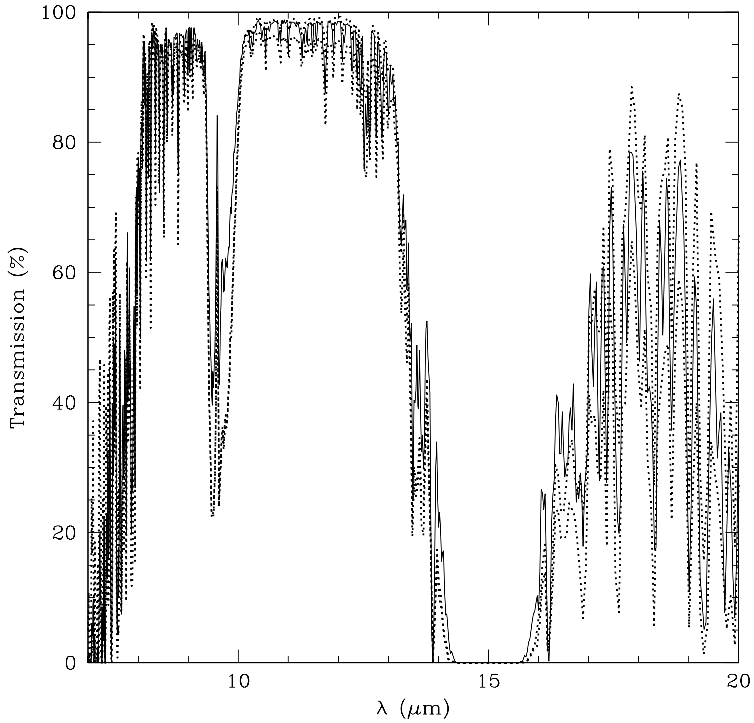

Fig. 4. Atmospheric transmission curves for SPM and Mauna Kea observatory sites calculated with MODTRAN. SPM curves (dotted lines) are for 1 mm (upper curve) and 3 mm (lower curve) water vapor contents, while the Mauna Kea curve (solid line) corresponds to 1 mm.

7. COLOR TERMS

The stars that define our photometric system (Table 2) are mainly of a neutral color (N-Q) ~ 0, as expected for the RJ portion of a stellar photospheric spectra. To correct for this limitation, we have supplemented the initial list with a set of 29 *IRAS* sources with available low resolution spectra (LRS), that are bright ($F_{12} > 100$ Jy) in the mid-infrared and cover a wide range of colors. We acknowledge that LRS spectra are not intended for absolute photometric calibration, but are believed to be accurate for comparing spectral distribution shapes (Cohen, Walker, & Witteborn 1992b).

The LRS spectra cover the range 7 to 23 μm in two sections, one running from 7 to 13.6 μm and the other from 10.6 to 23 μm. As the fluxes in the overlap region do not always coincide, we shifted the longer wavelength section of the spectra to match the shorter wavelength section, so that the differences in the overlap region are minimized.

The resulting spectra were further divided by the necessary factor to correct for the fundamental SiO band absorption of α Tau near 8 μm (as given in Cohen et al. 1992b).

The LRS sources were observed with CID-BIB in two runs, June 11, 2003 and November 10–12, 2005, under photometric conditions. The results are presented in Table 10. The observed fluxes were calibrated with the photometric system described in the previous section and are given in Jy. The corresponding *IRAS* LRS mean fluxes were determined from the LRS spectral data, integrating over the SPM-MIR filter system response as outlined by Eq. 3. Additionally, LRS fluxes for each source were corrected by a global factor g_{IRAS} (see Table 10) to simultaneously match the CID-BIB fluxes in all narrow-band filters. That is, for each source, g_{IRAS} is the factor that minimizes the square difference given by

$$\sum_{i=1}^{N_{filter}} \Big[\frac{F_{CID}(\lambda_i) - g_{IRAS}F_{IRAS}(\lambda_i)}{\sigma_{CID}(\lambda_i)}\Big]^2 ,$$

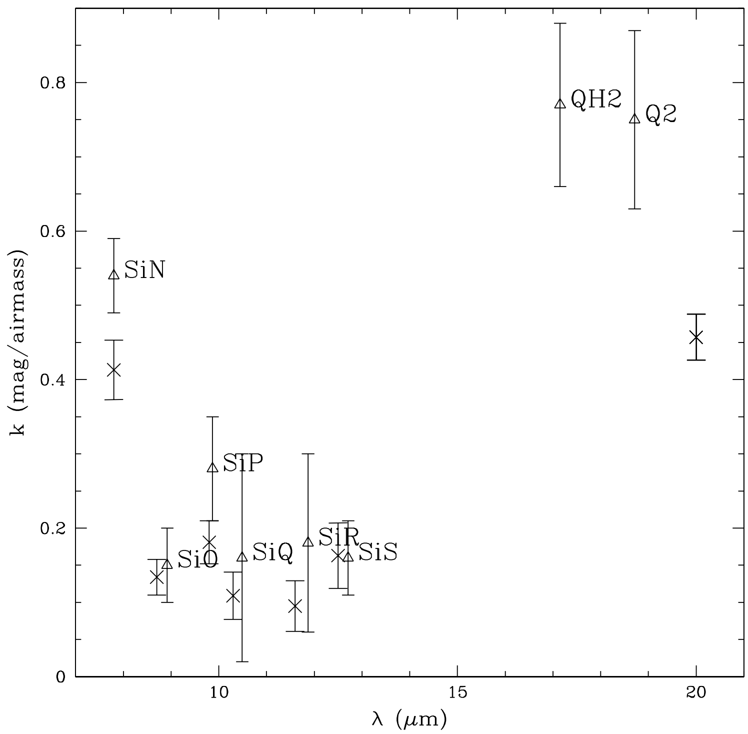

Fig. 5. Extinction coefficients (mag/air mass) for the SPM (triangles) and Mauna Kea (crosses) sites. The SPM values are also labeled with the corresponding CID-BIB filter name.

where σ_{CID} is given by the error in the CID photometry. In Figure 6 we show an example of this procedure. The LSR spectra of IRAS21419+5832, (μCep) shows well known silicate emission bands. It can be seen that the global correction g_{IRAS}=1.15 brings the IRAS flux quite close to the CID measurements. For extra comparison, we also show the ISO SWS spectrometer data for μCep (source 08001274) obtained from the Atlas at IRSA (IPAC, Caltech) (`http://irsa.ipac.caltech.edu/data/SWS/`) uniform catalog.

With the photometric results in the CID-BIB and the IRAS LRS systems we searched for possible color terms. These are explored through the correlations of the magnitude difference Δm for each filter, defined as

$$\Delta m_i \;=\; -2.5\,\log\,(\frac{F_{CID}(\lambda_i)}{F_{IRAS}(\lambda_i)})\,, \tag{10}$$

to the color $[8.9]-[18.7]$ given by Eq. 9. This particular color represents the largest wavelength base difference available, and avoids the large PAH feature al 7.7 μm and the silicate band at 9.7 μm.

Figure 7 presents the magnitude differences versus color for all observed sources in each filter.

We have calculated the probability that a set of straight lines describes the measured differences, according to the χ^2 distribution. We consider all lines that pass through the origin, that is, zero correction for zero color. We then evaluate the probability that the observed χ^2 should be as large as measured just by chance. The results are given in Table 11, where m_1 and m_2 represent the slopes that limit the range of solutions with a probability larger than 1/1000. The best slope is listed as m_{min}, and the probability that it should give rise to the listed χ^2 value is given as $P(m_{min})$. Also given is the probability that $m=0$ is an acceptable solution.

We note that for the SiP, SiQ, SiR and QH2 filters, the solution with a slope different from zero is significant and with a higher probability than that for $m=0$. Particularly, for the SiP filter the probability of $m=-0.03$ is 28 times larger than the probability for $m=0$. This would imply that we cannot exclude the probability that this filter requires a color correction given by

$$m_{[9.9]} \;=\; m^o_{[9.9]} \;+\; 0.03\,([8.9] \;-\; [18.7])\,, \tag{11}$$

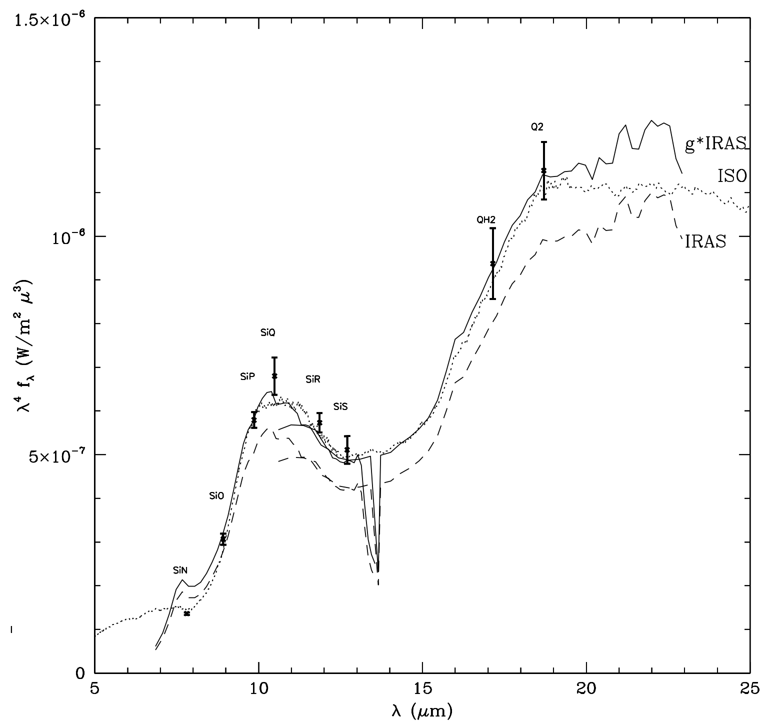

Fig. 6. LRS spectrum of IRAS21419+5832 (dashed line) is multiplied by g_{IRAS}=1.15 factor (solid line) to compare to CID measurements. Also shown for comparison is the ISO SWS spectrum of μCep (dotted line).

where the correction factor (0.03) represents the most probable value. We tested this result taking out seemingly outlying values; the two points that are higher up and to the right in the corresponding graph. The result holds, although the correction goes down to 0.02 instead of 0.03. We should point out that in doing this statistical test, we are not so firm in actually showing the existence of a color term, but in ruling out the possibility of a large color term. That is the reason to show the values of m_1 and m_2 that limit the probability of larger m values (larger than 0.05 in this case) to less than 1/1000.

With the same cautionary note, a similar correction would be required for the SiQ filter,

$$m_{[10.5]} = m^o_{[10.5]} + 0.03\,([8.9] - [18.7])\,. \tag{12}$$

The SiR and QH2 have almost the same probability for a solution with m = 0, so we think a color correction is not justified.

For the SiN and Q2 filters we get low values for the probability that any proposed straight line is an acceptable solution. This should then imply that a larger source of error is more significant than a color term, and that it masks our present possibilities to measure it. In Fig. 7 we also show the correction factor g_{IRAS} as a function of color. Surprisingly, it shows a tendency (r = −0.38) of being smaller for redder sources. This awkward behavior and its implications should be pursued further through additional observations and comparison to other photometric systems.

We have thus found that there may be color terms in at least two (SiP and SiQ) filters based on observations of sources as red as 4 mag in the ([8.9] – [18.7]) color. These are sources with rising spectral energy distributions even at 20 μm. At wavelengths longer than this, the composite response of the system must decay sharply. At 30 μm the quantum efficiency of the detector goes below 5%, the blocking filters transmission goes under 1% as does the atmospheric transmission. So any plausible red leak of the 10 μm window filters above 30 μm would be limited to less than 5×10^{-6}, which is insignificant for most applications.

TABLE 10

FLUXES OF IRAS LRS SOURCES

IRAS	CID[a]								IRAS LRS[b]								
source	SiN	SiO	SiP	SiQ	SiR	SiS	QH2	Q2	SiN	SiO	SiP	SiQ	SiR	SiS	QH2	Q2	g_{IRAS}
20077−0625	570.3	884.7	1057.0	1088.0	1060.0	968.0	1388.0	1482.0	654.5	977.6	1020.0	1049.0	1111.0	954.8	1248.0	1278.0	0.83
21318+5631	101.0	132.7	158.1	173.6	188.2	202.2	238.8	219.8	100.3	137.5	151.7	164.4	193.0	201.9	210.1	209.2	0.74
21381+5000	0.0	59.0	69.5	45.6	83.8	104.0	157.6	150.7	60.6	59.6	57.5	65.2	89.8	100.4	134.3	144.7	0.71
22176+6303	217.6	97.9	131.9	124.8	242.4	357.3	···	···	163.4	107.0	91.0	118.8	254.0	340.2	563.4	712.8	0.77
22177+5936	103.2	57.9	···	31.8	93.9	148.8	···	···	97.0	67.7	29.9	36.3	94.3	129.9	144.9	156.3	0.83
22480+6002	···	67.9	135.6	145.4	89.1	69.6	···	175.1	31.6	64.0	136.8	147.7	114.9	91.6	153.6	172.1	0.72
22512+6100	36.4	44.1	69.8	86.8	73.2	67.3	80.2	72.0	27.5	42.8	80.5	86.4	76.4	65.6	75.4	78.7	0.67
22525+6033	42.8	64.6	111.8	138.5	110.9	101.6	85.2	104.9	53.3	65.9	101.1	111.2	112.6	102.9	109.7	117.4	0.94
22556+5833	58.9	126.7	212.9	248.6	168.7	129.6	186.0	187.1	55.7	122.3	220.4	236.2	193.5	153.8	216.6	227.1	1.07
23166+1655	366.9	498.0	631.3	603.5	606.7	793.3	889.7	1057.0	369.4	517.9	613.6	645.6	691.5	740.1	830.1	786.6	0.99
23416+6130	104.9	213.6	453.2	504.3	339.3	259.6	432.5	498.5	124.7	212.2	428.1	460.6	348.9	269.2	450.0	499.2	0.96
01144+6658	34.9	51.4	68.2	72.8	83.4	96.7	144.3	142.2	37.4	55.7	63.3	68.8	85.7	94.2	115.5	117.4	0.65
01304+6211	118.1	55.8	33.6	32.5	79.2	139.4	139.2	155.2	80.9	60.0	24.7	29.3	77.7	111.5	126.2	133.8	0.32
02152+2822	84.5	112.2	102.1	108.8	112.9	115.4	···	68.4	84.2	101.5	104.1	113.9	121.5	104.6	100.2	97.4	0.89
02293+5748	89.5	116.5	139.5	129.7	140.2	153.3	···	128.6	86.9	114.6	118.9	128.8	146.7	136.8	129.7	126.9	0.84
04395+3601	91.2	195.2	291.5	305.5	348.5	378.3	855.9	882.4	139.8	220.4	286.5	315.6	368.9	426.2	777.4	890.8	0.92
05073+5248	280.1	365.8	399.1	412.9	411.3	353.4	420.0	440.2	230.9	339.4	397.4	414.5	420.3	356.6	498.9	525.2	1.26
05361+4644	89.7	125.5	155.7	145.7	145.8	138.2	174.6	158.8	82.8	116.8	136.7	142.8	146.9	139.1	167.7	177.7	0.79
06297+4045	86.7	182.1	243.8	261.7	205.8	144.6	170.5	165.5	97.2	164.9	222.2	228.4	205.3	169.0	216.4	227.6	1.87
21419+5832	744.2	1285.0	1987.0	2062.0	1358.0	1055.0	1062.0	1070.0	1095.0	1370.0	1975.0	1885.0	1272.0	992.8	1048.0	1072.0	1.15
17119+0859	···	398.8	547.8	···	···	336.2	371.6	···	216.6	356.4	553.7	561.8	427.2	324.5	409.1	436.2	1.01
18239−0655	···	182.0	168.4	···	···	162.3	105.1	···	167.3	181.8	174.9	190.1	207.4	176.4	136.8	132.7	0.93
18560+0638	236.6	178.2	127.2	147.2	235.0	287.8	344.8	373.7	210.2	184.9	114.7	138.4	253.1	296.7	339.1	347.3	1.02
18349+1023	250.3	402.2	572.6	691.0	461.5	359.3	423.5	431.0	264.8	396.4	541.0	552.2	452.8	368.8	373.0	385.2	1.28
17297+1747	477.9	436.1	452.3	464.6	446.5	427.2	363.4	348.7	425.6	443.0	461.1	480.4	476.6	447.5	403.3	385.7	1.13
18333+0533	232.3	243.0	219.7	221.5	252.5	248.6	290.3	319.2	156.1	214.9	216.9	231.5	265.1	239.6	336.1	357.9	1.02
18387−0423	110.4	187.8	301.6	332.2	281.2	229.4	289.8	325.8	127.7	179.8	289.0	310.7	285.9	240.6	280.4	301.9	0.71
18397+1738	842.7	723.1	693.5	750.7	775.9	591.4	379.9	338.0	694.3	729.2	699.6	744.5	753.5	571.5	397.2	367.7	1.08
18413+1354	116.4	198.8	284.6	298.3	214.3	160.2	166.9	179.7	113.0	185.1	282.5	285.7	216.9	168.6	201.1	205.7	1.01

[a]Fluxes are given in Jy.

[b]g_{IRAS} is the global factor applied to LRS integrated fluxes to coincide with the CID-BIB values.

TABLE 11

COLOR TERMS

Filter	m1	m2	m_{min}	$\chi^2(m_{min})$	N	$P(m_{min})$	$P(m=0)$
SiN	···	···	−0.03	162.19	22	0.0000	0.0000
SiO	−0.03	0.02	0.00	28.97	26	0.2653	0.2653
SiP	−0.05	0.00	−0.03	32.71	27	0.1708	0.0059
SiQ	−0.06	0.00	−0.03	30.09	24	0.1468	0.0063
SiR	−0.02	0.05	0.02	11.30	25	0.9867	0.8519
SiS	−0.02	0.01	0.00	42.02	27	0.0245	0.0245
QH2	−0.02	0.00	−0.01	36.91	16	0.0013	0.0010
Q2	···	···	0.03	80.96	20	0.0000	0.0000

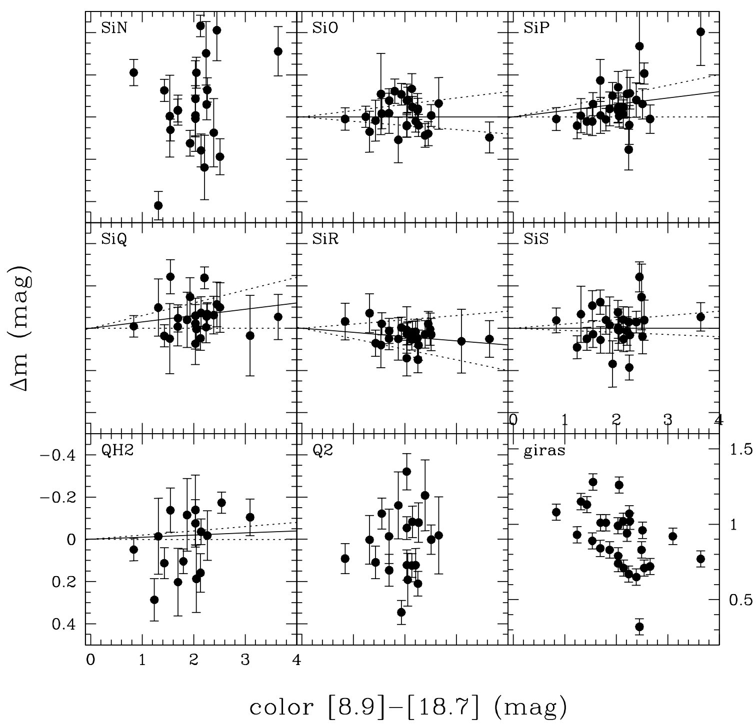

Fig. 7. Color terms. Magnitude difference Δm in some 10 μm and 20 μm window filters as a function of *IRAS* LRS color. Dots represent the observed differences. Solid line is the best χ^2 fit, and dotted lines limit the range of solutions with probability > 1/1000. The last panel (lower left), shows the g_{IRAS} (see § 7) factor (right axis) as a function of color.

We are indebted to an anonymous referee for a series of comments and suggestions that lead to a significant improvement of the present paper. We would like to thank the staff of the Observatorio Astronómico Nacional at San Pedro Mártir, for their valuable assistance in the observations. The CID-BIB is part of the infrared facilities operating at the Observatorio Astronómico Nacional in San Pedro Mártir, and was financed primarly through grants PACIME-CONACYT F325-E9211, CONACYT 1021PE, 36574E supplemented by DGAPA-UNAM 1N501694, 1N108696, 1N105400, 1N102803, and 1N104693.

REFERENCES

Berk, A., Bernstein, L. S., & Robertson, D. C., 1989, MODTRAN: A moderate resolution model for LOWTRAN7 (GL-TR-89-0122). Air Force Geophysics Laboratory, Bedford, Mass.

Cohen, M., Walker, R. G. Barlow, M. J., & Deacon, J. R. 1992a, AJ, 104, 1650

Cohen, M., Walker, R. G., Carter, B., Hammersley, P., Kidger, M., & Noguchi, K. 1999, AJ, 117, 1864

Cohen, M., Walker, R. G., & Witteborn, F. C. 1992b, AJ, 104, 2030

Cohen, M., Witteborn, F. C., Carbon, D. F., Davies, J. K., Wooden, D. H., & Bregman, J. D. 1996, AJ, 112, 2274

Cohen, M., Witteborn, F. C., Walker, R. C., Bregman, J. D., & Wooden, D. 1995, AJ, 110, 275

Cruz-González, I., Avila, R., Tapia, M. (Editors) 2003, "San Pedro Mártir: Astronomical Site Evaluation", RevMexAA (Serie de Conferencias), Vol. 19

Forbes, J. D., 1842, Phil. Trans., 132, 225

Golay, M. 1974, Introduction to Astronomical Photometry, Vol. 41, in the Astrophysics and Space Science Library (Dordrecht: Reidel)

Hiriart, D., Goldsmith, P. F., Skrutskie, M. F., & Salas, L. 1997, RevMexAA, 33, 59

Krisciunas, K., Sinton, W., Tholen, K., et al. 1987, PASP, 99, 887

Milone, E. F., & Young, A. T. 2005, PASP, 117, 485

Salas, L., Gutiérrez, L., Tapia, M., Cruz-González, I. et al. 2003, Proc. SPIE, 4841, 594

Sohn, E., Ruiz Schneider, E., Salas, L., Gutérrez, L., & Cruz-González, I. 2001, Proc. SPIE, 4454, 135

Tokunaga, A. T. 1986, IRTF Photometry Manual

Tokunaga, A. T, Simons, D. A., & Vacca, W. D. 2002, PASP, 114, 180

Tokunaga, A. T., & Vacca, W. D. 2005, PASP, 117, 421

Young, A. T., Milone, E. F., & Stagg, C. R. 1994, A&AS, 105, 259

Irene Cruz-González: Instituto de Astronomía, UNAM, Apdo. Postal 70.264, 04510 México, D. F., México (irene@astroscu.unam.mx)

Luis Salas and Mauricio Tapia: Instituto de Astronomía, UNAM, Apdo. Postal 877, 22860 Ensenada, B. C., México (mt, salas@astrosen.unam.mx).